Phase Modulated Circles in a Sunflower-type Circular Photonic Crystal with Ultra-small Mode Area and High-Q Cavity

Joy Bhattacharjee*, Ashfaqul Anwar Siraji*†, *Student Member, IEEE* and M. Shah Alam*†‡, *Senior Member, IEEE*
*Department of Electrical and Electronic Engineering
Bangladesh University of Engineering and Technology (BUET)
†Department of Electrical and Electronic Engineering
Northern University Bangladesh
Email: ‡shalam@eee.buet.ac.bd

***Abstract*—A modified sunflower type circular photonic crystal defect cavity consisting of 10 concentric circles is studied where the defect cavity is created by removing the central hole. The resonant characteristics of the CPC defect cavity with gradually shifted phase angle in successive hole circles are analyzed. The resonant transverse electric (TE) and transverse magnetic (TM) mode frequencies were calculated by 2D finite difference time domain (FDTD) method. The field profiles at resonant frequencies are calculated and mode areas ($\mathbf{A_m}$) are determined from both TE and TM mode profiles. It is found that temporal decay of field energy in the cavity is exponential. From the decay of the energy in the cavity, the quality factor (Q) of the PC cavity is determined. Finally the impact of phase modulation on Q and $\mathbf{A_m}$ of the designed CPC defect cavity is examined.**

***Index Terms*—Phase Modulation, Circular Photonic Crystal, High-Q, Finite Difference Time Domain.**

I. Introduction

One avenue of active research in lightwave technology is Photonic crystal devices. Photonic crystal is an artificial medium that obtains a complete photonic bandgap (PBG) in frequency where the electromagnetic wave propagation is prohibited in all directions. This prohibition allows for controlling the propagation of light in a selected frequency range. In order to trap light, a defect cavity can be created in PC where a strongly localized defect state appears. Depending on the physical properties of the PC and the defect cavity, a resonant mode of the cavity can be identified. Defect cavities in PC slab, where the confinement in the slab plane is due to PBG and that in the perpendicular direction by total internal reflection (TIR) [1], are specially attractive for planar photonic applications [2, 3]. For example, a band-edge laser with small active area using a slab cavity has been designed [2] while a high resolution spectrometer based on a series of PC slab cavity has been proposed [3].

Circular optical resonator plays a niche role in optical communication systems including low threshold lasers [4], filters, modulators [5], nonlinear optics [6] etc. Most circular resonators exhibit high Q, small mode area and good confinement when their dimension are large. However, when reduced dimension is required, disk radius is decreased which increases bending losses from TIR and degrades the Q [4]. PBG structures like circular grating resonator (CGR) and annular circular resonator (ACR) is proposed for their ability to reduce the bending losses [4, 6]. But they are unsuitable for several applications because of their discontinuous structures [4]. Circular photonic crystal (CPC) cavity has been proposed as an alternative to these discontinuous structures [5, 6, 7].

CPCs are designed with successive concentric circles with three different arrangements of airholes, viz. rectangular lattice, triangular lattice and sunflower lattice. The sunflower type of lattice has linearly increasing number and constant angular size of holes [8]. This lattice is highly symmetric with infinite number of symmetry planes. As a result, isotropic PBG can be easily found in CPCs using this type of lattice [4]. Moreover, it can better support highly confined whispering gallery mode (WGM) [4, 5]. The circular structure of the CPC offers several advantages for cavity designing, for example, it allows for optimal tailoring of the cavity size and the reflector periodicity [9]. Hence, sunflower type CPC is very suitable for designing CPC cavity. Since CPC cavities need to be integrated with planar photonic circuits, we consider a CPC slab cavity.

Quality factor (Q) improvement of a slab cavity is difficult because the confinement of light in the perpendicular direction is imperfect [10]. Several methods have been adopted to increase Q of a PC slab cavity. We have demonstrated that applying space modulation on a defect cavity can increase the Q [11]. We have also demonstrated that incorporating a slot waveguide with in the cavity can increase the Q [12]. An analogue to space modulation in case of the CPC can be phase modulation, where the phases of the successive airhole circles are harmonically changed. To the best of our knowledge, such an improvement scheme has not been reported in case of CPC slab cavity so far.

In this work, we have presented a two dimensional (2D) finite difference time domain (FDTD) analysis of a CPC slab cavity incorporating phase modulation. Since the structure is highly symmetric with local periodicity, both transverse electric (TE) and transverse magnetic (TM) mode of the 2D geometry has been considered. We have calculated the resonant wavelengths of both TE and TM modes for different extent of phase modulation. For the resonant wavelengths, the resonant profile of the electric field (for TM mode) and magnetic field (for TE mode) has been calculated. Then the quality factor (Q) and mode area (A_m) for the resonant modes have been calculated. Finally, the impact of phase modulation

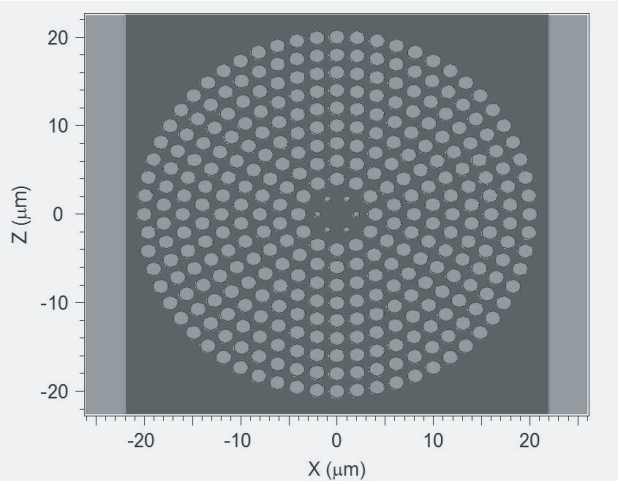

Fig. 1: Structure of Circular Photonic Crystal Cavity, the radius of the airholes is .8μm, the number of the rings is 10, the radial distance of the holes is 2.1μm and the refractive index of the background slab is 3.4.

on the resonant characteristics of the CPC cavity is elucidated.

II. Cavity Design

As described in [9], a hexagonal lattice can be deformed by stretching the lattice structure or by changing the angle ϕ between the two lattice vectors without changing the bandgap. It has been shown that even if we stretch or shear a hexagonal lattice, the complete bandgap remains around $a/\lambda = 0.42$ [9]. Hence, the circular photonic crystal has a forbidden frequency band.

The arrangement of holes in the designed CPC cavity is shown in Fig. 1. The distance between holes is kept constant on each concentric circle. A six-fold symmetric CPC is used as an prototype previously demonstrated by Horiuchi *et al.* [7]. The holes are arranged in the form of concentric circles with radial distance,i.e., distance between successive circles, $d = 2.1\mu$m and radius of airholes, $r = 0.8\mu$m on a slab of refractive index $\eta = 3.4$. The numbers of holes in successive circles increases linearly. The positions of holes in the xz plane are given by,

$$\begin{aligned} x &= dNsin(\theta_{pattern} + \theta) \\ z &= dNcos(\theta_{pattern} + \theta) \end{aligned} \tag{1}$$

where d is the radial distance, N is the number of concentric circles. The angle $\theta_{pattern} = \frac{2m\pi}{6N}$, where m is an integer from 1 to 6N and θ is phase angle.

In this work, we considered a circular photonic crystal consisting of 10 concentric circles. The circles are indexed according to their position from the center. The central hole is eliminated to form a defect cavity. The radius of the airholes in the 1st circle around the cavity is reduced for better confinement of light in the cavity and its radius is, $r_1 = r \times .2$.

We examined three different structures derived from the same CPC structure. At first, the phase angle(θ) for the air holes of the 1^{st} circle is set to $\pi/6$. This CPC structure is denoted by CPC_1. Then continuing from the previous structure, θ is set to $\pi/4$ for the air holes of the 2^{nd} circle. This CPC structures is denoted by CPC_2. Finally, continuing from the previous structure, θ is set to $\pi/8$ for the air holes of the 3^{rd} circle. This CPC structures is denoted by CPC_3. These three CPC defect cavities are analyzed in the subsequent sections.

III. Simulation Details

The Cavity is excited with a large range of frequencies to find the resonant frequency. The excitation propagates freely in the cavity. We get sharp peak for resonant frequencies in the frequency spectrum because resonant frequencies excite the cavity and their energy decay very slowly. Most other frequencies do not excite the cavity and their energy leaves the cavity quickly.

We used 2-D FDTD method to solve the Maxwell's equations. The FDTD method reduces the vector cross equations into difference equations. Two of those six equations are given below:

$$\begin{aligned} H^{n+1/2}_{x(i,j,k)} = H^{n-1/2}_{x(i,j,k)} &+ \frac{\Delta t}{\mu \Delta z}(E^n_{y(i,j,k)} - E^n_{y(i,j,k-1)} \\ &- \frac{\Delta t}{\mu \Delta y}(E^n_{z(i,j,k)} - E^n_{z(i,j-1,k)} \end{aligned} \tag{2}$$

and

$$\begin{aligned} E^{n+1}_{x(i,j,k)} = E^n_{x(i,j,k)} &+ \frac{\Delta t}{\varepsilon \Delta y}(H^{n+1/2}_{z(i,j+1,k)} - H^{n+1/2}_{z(i,j,k)} \\ &- \frac{\Delta t}{\varepsilon \Delta z}(H^{n+1/2}_{y(i,j,k+1)} - E^{n+1/2}_{y(i,j,k)} \end{aligned} \tag{3}$$

The most common method to solve these equations is based on Yee's mesh and computes the $\mathbf{E}$ and $\mathbf{H}$ field. As we performed calculations for the Transverse Electric(TE) and Transverse Magnetic(TM) modes, we calculated the $\mathbf{H}_y$, $\mathbf{E}_x$ and $\mathbf{E}_z$ components of the TE mode and the $\mathbf{E}_y$, $\mathbf{H}_x$ and $\mathbf{H}_z$ components of the TM mode. We used 16 grid points per micrometer, which provided sufficiently converged results. To have sufficient frequency resolution, we used time step $\Delta t = 1.0417 \times 10^{-16} s$ which is smaller than the Courant limit ($1.473 \times 10^{-16} s$).

To excite the structure using an impulse, we need to define an initial launch condition. The excitation is composed of both spatial and temporal components and can be expressed as:

$$\phi_L(\mathbf{r}, t) = e^{\frac{-(x^2+z^2)}{a^2}} \delta(t - t_0) \tag{4}$$

where a= width/2= 5μm/2= 2.5μm and $\delta(t - t_0)$ is a delta function in the time domain.

The excitation can be represented as a sum of individual excitations and can be expressed by the following equation:

$$\phi_L(\mathbf{r}, t) = \sum_i \phi_i(\mathbf{r}, t) \tag{5}$$

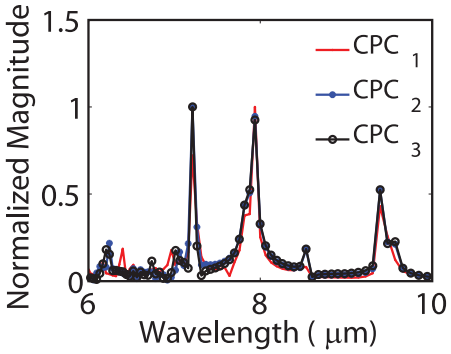

(a)

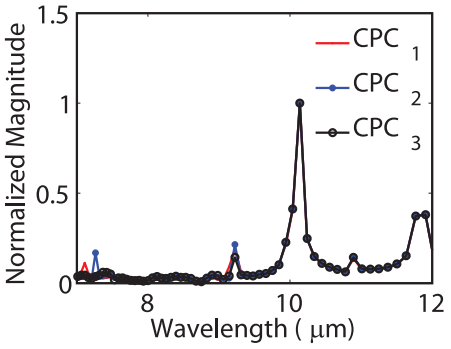

(b)

Fig. 2: (a) Normalized energy spectra for TE mode in case of CPC_1, CPC_2, CPC_3. CPC_1 shows TE resonance at λ_r =7.97 μm. CPC_2 and CPC_3 both shows two resonant wavelengths. The TE resonances of CPC_2 are at λ_r =7.41 and 8.03 μm, respectively and those of CPC_3 are at λ_r =7.37 and 8.08μm, respectively (b) Normalized energy spectra for TM mode in case of CPC_1, CPC_2, CPC_3 showing resonances at λ_r = 10.19, 10.09 and 10.17 μm, respectively.

The individual excitation $\phi_i(\mathbf{r}, t)$ is defined as:

$$\phi_i(\mathbf{r}, t) = \sqrt{P_i} f_i(\mathbf{r}) g_i(t) e^{i\phi_i t} \tag{6}$$

where P_i and ϕ_i are the power and phase of the excitation, and $f_i(\mathbf{r})$ and $g_i(t)$ are the spatial and temporal components of the excitation. A field source is used for excitation as an incident beam within the simulation domain.

Since the structure is finite, we used Perfectly Matched Layers (PMLs) of $= 0.5\mu$m surrounding the cavity to simulate open boundaries. This allows the energy incident on the boundary to leave the structure.

IV. Results

A. Resonant frequency

To obtain the resonant frequency of the cavity, we excited the defect cavity by a broadband impulse. The impulse propagated freely and it's evolution in the time domain was recorded. The time response was calculated by solving the Maxwell's questions for $\mathbf{E}_y$ component of the TM mode and $\mathbf{H}_y$ component of the TE mode with the initial conditions specified in (4). The frequency spectrum was calculated by using Fast Fourier Transform (FFT). Since we need to know the relative strength of the energy in the cavity with respect to excitation wavelength, the spectrum is normalized. The normalized spectra are shown in Fig. 2. As the structure only has local periodicity and the symmetry has been broken, several resonant modes of differing symmetry is possible. Hence the frequency spectrum consists of several peaks. The presence of sharp peaks indicates that the electromagnetic radiation of the mentioned wavelengths stays within the cavity far longer than radiations of other wavelengths. The presence of side lobes of comparable strength leads to spectral impurity. The sharp resonant peaks are isolated with significantly less side lobes. The resonant wavelengths (λ_r) and normalized frequencies (d/λ_r) for the studied cases are given in Table I.

From Table I and Fig. 2(a), we can see that there are two resonant TE modes in CPC_2 and CPC_3. For CPC_2, the frequency spectrum has sharp peaks at $\lambda = 7.41\mu$m and 8.026μm, separated by 616 nm. For CPC_3, the frequency spectrum has sharp peaks at $\lambda = 7.36\mu$m and 8.079μm, separated by 719 nm. From the difference we can say that the resonant TE modes are not degenerate modes separated by mesh coarseness.

The resonant wavelengths are: for TE mode $\lambda_r = 7.96 \sim 8.08\mu$m, shown in Fig. 2(a) and for TM mode $\lambda_r = 10.09 \sim 10.19\mu$m, shown in 2(b). The resonant wavelength of the TE mode canges by as much as 7% when phase modulation is applied. However, the resonant wavelength of the TM resonant mode changes only by 0.2%.

TABLE I: Values of Resonant Wavelengths, Normalized frequencies, Mode Area and Mode area/Device area

	Mode	$\lambda_r(\mu$m)	d/λ_r	$A_m/(\lambda_r/\eta)^2)$	$A_m/A_d(10^{-3})$
CPC_1	TE	7.97	0.26	1.31	3.1
	TM	10.19	0.20	1.78	6.8
CPC_2	TE	7.41	0.28	1.75	3.6
		8.03	0.26	2.11	5.0
	TM	10.09	0.21	2.00	7.5
CPC_3	TE	7.37	0.29	2.12	4.3
		8.08	0.26	1.28	3.1
	TM	10.17	0.21	0.16	6.9

B. Spatial Confinement

Once the resonant frequencies were known, we calculated the field profile of the cavity at those frequencies. The magnitude profiles $\mathbf{H}_y$ for the TE mode and the electric field magnitude profiles $\mathbf{E}_y$ for the TM mode at corresponding normalized frequency for three different patterns of CPCs are shown in Fig. 3. Because of circular crystal structure, the field patterns are also circular. Most of the energy is confined in the dielectric between the smaller holes of the first circle. The highest amount of energy remains in the air hole at the center. As the holes in the second circle are comparatively bigger with less dielectric around them, significantly less energy is leaked to the second circle. The energy in the dielectric between the outer circles is negligible.

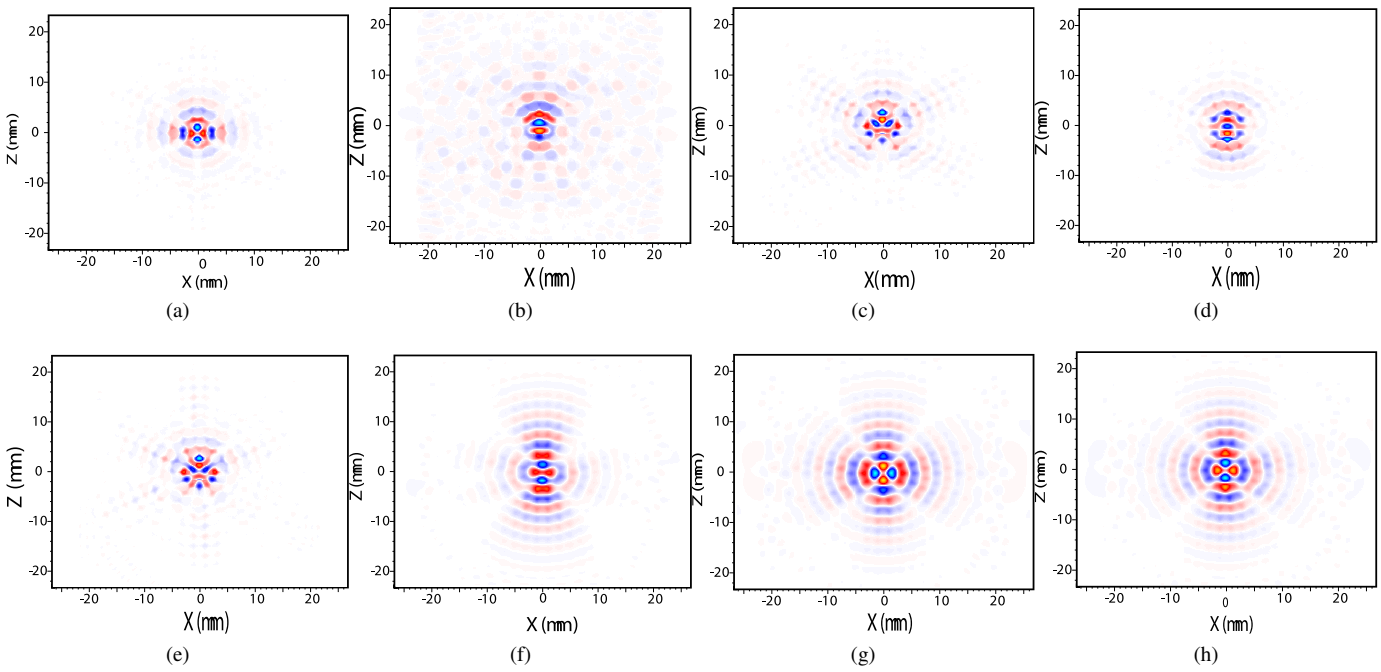

Fig. 3: Calculated resonant field profiles at respective normalized frequencies for the studied cases. (a) The H_y field profile of the resonant TE mode of CPC_1, (b) The H_y field profile of the first resonant TE mode of CPC_2, (c) The H_y field profile of the second resonant TE mode of CPC_2,(d) The H_y field profile of the first resonant TE mode of CPC_3, (c) The H_y field profile of the second resonant TE mode of CPC_3, (f) The E_y field profile of the resonant TM mode of CPC_1, (g) The E_y field profile of the resonant TM mode of CPC_2 and (h) The E_y field profile of the resonant TM mode of CPC_3

As two resonant TE modes for CPC_2 and CPC_3 each were found, we have eight mode profiles. The first resonant TE mode at $\lambda_r = 7.41\mu$m for CPC_2 is leakiest of all, shown in Fig. 3(b). TE mode for CPC_1, shown in 3(a) and TM modes for all three types of CPCs we studied, shown in Fig. 3(f), 3(g) and 3(h), are whispering-gallery type [14]. The radiated power depends only on the wave vector components located within the light cone. Therefore, the reduction in radiation loss and the improvement of Q factor can be achieved by suppressing the Fourier components within the light cone or by redistributing them outside the light cone.

By using following formula, we calculated mode areas(A_m) for TE and TM modes.

$$A = \frac{(\int F^2 dA)^2}{\int F^4 dA} \tag{7}$$

where F = Field distribution. Mode areas(A_m) and ratios of mode area(A_m) to device area(A_d) for three patterns are shown in Table I. The smallest mode area is, A_m = $1.28(\lambda_r/\eta)^2$ for CPC_3. From Table I, the mode area and the ratio of mode are to device are for all the considered cases can be observes. When phase modulation is applied to the first circle only, the mode are for the TE and TM mode are $1.31\times(\lambda/eta)$ and $1.78\times(\lambda/eta)$ respectively. When the extent of phase modulation is increased, the mode area of the resonant modes monotonically increase. This indicates the as phase modulation is applied to greater extent, the spatial confinement in the device plane becomes gentler.

C. Temporal Confinement

In many structures such as photonic crystal cavities or micro-ring resonators, the states in which energy is stored in the cavity are not true modes of the system, but finite-lifetime resonances. In the event that a given spectral resonance is reasonably isolated from any others, the stored energy decays exponentially in time and exhibits a Lorentzian line profile [15]. Quality factor of a cavity is defined as the decay of energy per cycle. Thus, quality factor can be written as,

$$Q = \frac{2\pi}{\alpha\lambda_r}, \tag{8}$$

where α is the temporal energy decay constant. To calculate the decay constant, we excited the cavity with the resonant mode profile and calculated the total energy density with time. The energy density is the sum of electric and magnetic field energy density given as:

$$S(t) = \frac{1}{2}\int_V \left(\epsilon(\mathbf{r})|\mathbf{E}(t)|^2 + \mu|\mathbf{H}(t)|^2\right) dV. \tag{9}$$

The envelope of the energy in the cavity with respect to time is shown Fig. 4. From the figure, we can conclude that the decay of energy in the cavity is exponential. We fit the envelope with an exponential of the form

$$U = U_0 E^{-\alpha t}, \tag{10}$$

where U_0 is the maximum of the energy, here normalized to 1.By inserting the calculated α into (8), we can obtain the quality factor, since λ_r is already known.

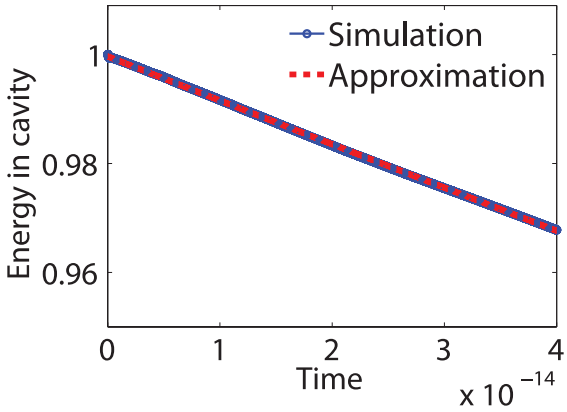

Fig. 4: The decaying temporal profile of the total energy in the cavity for the TE mode. The decay can be approximated as a decaying exponential.

Different values of Quality Factor (Q) for three different patterns of CPCs we studied are shown in Table II.

TABLE II: Quality Factors for three types of CPCs

	Mode	Q
CPC_1	TE	2.16×10^4
	TM	1.16×10^4
CPC_2	TE	0.17×10^4
		1.57×10^4
	TM	1.47×10^4
CPC_3	TE	1.26×10^4
		4.55×10^4
	TM	1.44×10^4

The phase modulation technique we approached results in reducing field intensity of within the light cone. Hence out-of-plane losses are reduced and out-of-plane Q is improved resulting in improving the overall Q. The highest quality factor for our work is, Q = 4.6×10^4 for CPC_3 at its second resonant TE mode at 8.079μm. As the smallest mode area is for it also, we get the highest Q/A ratio for it and is equal to $3.55(\eta/\lambda_r)^2$. As stated earlier, the first resonant TE mode at 7.41μm for CPC_2 is the leakiest, we get the lowest Q(=1764) for it as expected.

As the phase modulation technique improves out-of-plane Q by reducing out-of-plane losses, further modulation can be approached. As we get increasing value of Q for consecutive phase modulation, modulation of other circles in CPC may result in higher Q and smaller mode area. Phase modulation with other harmonic patterns of phase angle may be approached for better results.

In order to get a perspective on the result we provide a comparison with previously reported quality factors in Table III. The calculated quality factor in this work compares well with the one calculated in [4] and [13].

TABLE III: Comparison of the computed quality factor with previously reported values.

Reference	Quality Factor (Q)
Siraji *et al.* [9]	1.3×10^3
Errico *et al.* [5]	2×10^3
Siraji *et al.* [12]	6×10^3
Lee *et al.* [4]	1×10^4
This work	4.6×10^4
Minkov *et al.* [13]	5.4×10^4

V. Conclusion

We have studied the effect of phase modulation on the resonant characteristics of a defect cavity in circular photonic crystal using FDTD method. The defect was created by removing the center circle. Then the 1^{st} circle containing 6 concentric holes, was rotated by $\pi/6$ so the holes in that circle shifted by corresponding x,y positions. The magnetic field energy profile of the resonant TE mode and electric field energy profile of the resonant TM mode were calculated. The exponential decay of energy away from the cavity was calculated and shown as a measure of the spatial confinement of energy in the cavity. The decay of energy in the resonator was also calculated to be of exponential. From the exponential decay rate, the quality factor of the resonator was calculated. Then the 2^{nd} circle containing 12 concentric holes and the 3^{rd} circle containing 18 concentric holes, were rotated by $\pi/4$ and $\pi/8$ respectively. Similar simulations were conducted for each of them. We got several values of resonant wavelengths, Q factors and modal areas and compared them. The small A, high Q CPC cavity or CPC structures having cavity with high Q/A ratio are specially attractive for laser, Bio-molecular sensing etc.

References

[1] Rui Hao, Zhiquan Li, Guifang Sun, Liyong Niu, Yuchao Sun, "Analysis on photonic crystal fibers with circular air holes in elliptical configuration," *Optical Fiber Technology*, vol. 19, no. 5, pp. 363–368, Oct. 2013.

[2] D.-U. Kim, S. Kim, J. Lee, S.-R. Jeon, and H. Jeon, "Free-standing GaN-based photonic crystal band-edge laser," *IEEE Photonic Technology Letters*, vol. 23, no. 20, pp. 1454–1456, Oct. 2011.

[3] X. Gan, N. Pervez, I. Kymissis, F. Hatami, and D. Englund, "A high-resolution spectrometer based on a compact planar two dimensional photonic crystal cavity array," *Applied Physics Letters*, vol. 100, no. 23, pp. 231104,231104–4, June 2012.

[4] Po-Tsung Lee, Tsan-Wen Lu, Jyun-Hao Fan, and Feng-Mao Tsai, "High quality factor microcavity lasers realized by circular photonic crystal with isotropic photonic bandgap effect," *Applied Physics Letters*, vol. 90, no. 15, Article ID 151125, Apr. 2007.

[5] V. Errico, A. Salhi, C. Giordano, M. DeGiorgi, A. Passaseo, M. DeVittorio, "High-Q factor single mode circular photonic crystal nano-resonator," *Superlattices*

and Microstructures, vol. 43, no. 5–6, pp. 507–511, Sept. 2007.

[6] Xufeng Zhang, Xiankai Sun, and Hong X. Tang, "A 1.16-m-radius disk cavity in a sunflower-type circular photonic crystal with ultrahigh quality factor," *Optics Express*, vol. 37, no. 15, pp. 3195–3197, Aug. 2012.

[7] N. Horiuchi, Y. Segawa, T. Nozokido, K. Mizuno, and H. Miyazaki, "Isotropic photonic gaps in a circular photonic crystal," *Optics Letters*, vol. 29, no. 10, pp. 1084–1086, May 2004.

[8] D. Chang, J. Scheuer, and A. Yariv,"Optimization of circular photonic crystal cavities – beyond coupled mode theory," *Optics Express* vol. 13, no. 23, pp. 9272–9279, Nov. 2005.

[9] Ashfaqul Anwar Siraji, M. Shah Alam, and Samiul Haque, "On the confinement of photons in a curvilinear lattice photonic crystal cavity," *International Conference on Electrical & Computer Engineering(ICECE)*, pp. 510-513, Dec. 2012.

[10] Tang, Lingling, Yoshie, Tomoyuki, "High-Q hybrid 3D-2D slab-3D photonic crystal microcavity," *Optics Letters*, vol. 35, no. 18, pp. 3144-3146, Sept. 2011.

[11] A. A. Siraji, M. S. Alam, and S. Haque, "Impact of space modulation on confinement of light in a novel photonic crystal cavity on ferroelectric barium titanate," *Journal of Lightwave Technology*, vol. 31, no. 5, pp. 802–808, Mar. 2013.

[12] A. A. Siraji and M. S. Alam, "A tunable photonic double heterostructure cavity on ferroelectric barium titanate," *IEEE Photonics Technology Letters*, vol. 25, no. 17, pp. 1676–1679, July 2013.

[13] M. Minkov, U. Dharanipathy, R. Houdr, and V. Savona, "Statistics of the disorder-induced losses of high-Q photonic crystal cavities," *Optics Express* vol. 21, no. 23, pp. 28233–28245, Nov. 2013.

[14] Han-Youl Ryu, Masaya Notomi, Guk-Hyun Kim and Yong-Hee Lee, "High quality-factor whispering-gallery mode in the photonic crystal hexagonal disk cavity," *Optics Express*, vol. 12, no. 8, Apr. 2004.

[15] J.D. Joannopoulos, S.G. Johnson, J.N. Winn, and R.D. Meade, *Photonic Crystals: Molding the flow of light*, 2nd Ed. Princeton University Press, 41 William Street, Princeton, New Jersey, Copyright 2008.